How the high-volume evacuation alters the flow-field and particle removal characteristics in the mock-up dental clinic

Xiujie Li [a], Cheuk Ming Mak [a], Kuen Wai Ma [a], Hai Ming Wong [b, *]

[a] Department of Building Services Engineering, The Hong Kong Polytechnic University, Hung Hom, Hong Kong
[b] Faculty of Dentistry, The University of Hong Kong, Pok Fu Lam, Hong Kong Island, Hong Kong

ARTICLE INFO

ABSTRACT

The exposure risk of droplets and aerosols emitted from the oral cavity to the dental professionals and patients has received more attention especially the ongoing outbreak of COVID-19. The aim of this study is to address the question about how the use of the high-volume evacuation (HVE) alters the risk profiles compared with the situation only personal protective equipment (PPE). The risk profiles of the different situations were analyzed in terms of droplet velocity, flow field characteristics, and particle removal efficiency. The ultrasonic scaling with suction was performed in the mock-up experimental dental clinic, and the instantaneous moment when the HVE acted on the droplets was visualized using a laser light scattering technique. From the results of the velocity profiles, the hypothesis about the moderate effect of the HVE on high-velocity small droplets near the mannequin's mouth had been firstly proven in this study. The suction can be characterized as low-threshold equipment to bring substantial benefits to reduce the area of the contaminated region. Once the cooperation of suction, the pair of vortexes that were in the face shield area of the dental professional would be eliminated, removing the high-level contaminated region near the breathing area of dental professionals. Compared with the low and medium volume evacuation, the particle removal efficiency of the HVE was more stable at 60%. The research will provide references to the HVE recommendation in the dentistry clinical practice guidelines.

1. Introduction

The ongoing COVID-19 pandemic has significantly affected the provision of medical and dental services, which greatly damages the human health and well-being of urban dwellers [1,2]. Owing to the potential transmission by the emitted droplets and aerosols, the dental professionals who are in close proximity to the oropharyngeal region are always at a high risk of cross-infection [3,4]. In Hong Kong, routine dental services had been suspended at the beginning of 2020 [5]. With increasing people begin to get vaccinated, the restoration of dental services is in the process all around the world.

The main infection pathways of SARs-CoV-2 are airborne and direct contact [6,7]. The airborne transmission occurs through the droplets and aerosols expelled by coughing, breathing, sneezing, and speaking [7,8]. The direct contact infection usually occurs when contacting contaminated surfaces and then touching the eyes, nose, and mouth [8, 9]. It has been indicated that the SARs-CoV-2 can remain viable in the air for at least 3 h [10]. The characteristics of persistent adherence to the various surface, a maximum of 9 days, should also be treated carefully

[11]. The above transmission characteristics pose a high infection risk for the medical staff and close person.

Since the oral mucosa, especially the salivary glands, is the most common receptor in the virus-cell interaction [12,13], this suggests that the droplets and aerosol generated during the dental procedures could also contain SARs-CoV-2 and thereby transmit the virus to the dentists and dental surgery assistants [14,15]. Droplets in various sizes could be generated during dental care treatment procedures. The distinction threshold between the aerosols and droplets have been modified from the historical 5 μm to 100 μm, considering the different aerodynamic behaviors [16]. The large droplets refer to the particle size over 100 μm. In the dental surgery environment, several methods have been employed to investigate the particle size distribution, like particle counter [17], aerodynamic particle sizer [18], and laser light scattering method [19]. During ultrasonic scaling, the particle size ranging from 5 μm to 300 μm was identified by the laser light scatting method [19]. The large droplets are difficult to be suspended in the air and are airborne only briefly [20, 21]. The transmission may occur when the large droplets expelled from the infectious individuals are directly on the mucus of susceptible

* Corresponding author.
  E-mail address: wonghmg@hku.hk (H.M. Wong).

subjects. In a few seconds, the droplets would begin to evaporate, and the size becomes smaller. The formed droplet nuclei have the potential to keep airborne or re-suspended as dust particles [22,23]. Therefore, the droplets and aerosols could be the potential source of infection transmission during dental care treatment procedures [24].

A field experiment in hospitals had found that the SARS-CoV-2 aerosols were mainly in two size ranges: the submicrometric region (0.25–1.0 μm) and the supermicrometre region (>2.5 μm) [25]. Besides, the SARS-CoV-2 had also been retrieved from the particulate matter (PM 10) in northern Italy [26]. Since most previous studies focused on the sample viral RNA instead of virus infectivity, whether the virus with infectious in these particles was still not identified. Additionally, the correlation between the potential viral load and the dental aerosols also needs further research [27]. Although several studies have demonstrated the high-contaminated region by detecting the presence of microbiota [28–30], the source of bacteria and SARS-CoV-2 detection in the dental surgery environment was still not well-investigated [31]. A recent field experiment demonstrated that the saliva contributed to a median of 0% of aerosol microbiota, and the dental irrigant, not the saliva, was the predominant source of airborne microbiota [32]. The discovery may validate the report of low infection rates of dental professionals [33]. Further research in the SARS-CoV-2 detection and the evaluation of mitigation measures in the dental surgery environment would help the restoration of the global dental services.

The high-volume evacuation (HVE) has been recommended in the dentistry clinical practice guidelines at the beginning of the pandemic as one mitigation measure [34,35]. The HVE is one type of suction device to draw a large volume of air and even droplets. This equipment could also cause some dental environmental noise [36–38]. However, the effect of these mitigating measures such as suction and ventilation is not well understood or explored (Epstein et al., 2020). Although some research studies evaluated the performance of the HVE by measuring the concentration of suspended particles [17,39,40], they were still limited to the number of sampling points and devices calibration. Recently, Balanta-Melo et al. measured the volume fraction of aerosol particles under 10 μm in the dental operating room and found that the HVE could reduce the generated particles, but not for all of them [41]. The finding was in line with Holliday's hypothesis that the effect of HVE on large droplets or high-velocity small droplets was moderate [27]. Besides, the question about how the use of the HVE alters the risk profiles compared with the situation of only personal protective equipment (PPE) is still unanswered. To complement the above research gaps, this study evaluated how the HVE shifts the risk profiles during ultrasonic scaling by analyzing the performance of the HVE from the droplet velocity, flow field characteristics, and particle removal efficiency.

Several methods have been employed to analyze the performance of the HVE, like luminescent tracer [42], bacteria culture methods, and even visual chromatic change detection [39,43]. However, the above three methods could only obtain the settled information like the area of contaminated regions, without measuring the velocity distribution of expelled droplets and even the flow-field characteristics. Although the particle concentration could be supplemented by the air sampler, the limited information (only concentration) was not enough for the complete evaluation of risk profile altering. Recently, the visualization method with laser scattering has been widely adopted in various disciplines to analyze the characteristics of velocity [44] and flow field [45]. In this study, the laser scattering methodologies have been adopted to visualize how the HVE acted on the droplets generated during ultrasonic scaling and further analyze the altering of risk profiles.

Therefore, the main purpose of this study is to quantitively answer how the use of the HVE alters the risk profiles in comparison with the situation where only masks, face shields, and other PPE by analyzing the performance of the HVE. In Section 2, the experimental design and analysis methods were described. The performance of the HVE was evaluated by analyzing the droplet velocity, flow field characteristics, and particle removal efficiency in Section 3. The discussion and main

conclusion of the experiment were presented in Section 4 and Section 5, respectively.

2. Materials and methods

2.1. Experimental design

The study was conducted in a mock-up dental clinic with dimensions of 3.6 m length x 2.7 m width x 2.3 m height. The room air temperature of the clinic was maintained to be $23 \pm 0.5°C$ during the experiment. The relative humidity was not controlled but in the range of 50%–60%. The square supply and exhaust diffusers (20 cm × 10 cm) were installed on both sides of the long axis of the ceiling, keeping the 6 air changes per hour (ACH). The experiment mimicked the typical ultrasonic scaling procedure on the vestibular side of the mandibular central incisor of a mannequin. The vibration rate and fixed water supply rate of the scaler tip were 30 kHz and 50 ml/min, respectively. Besides, the suction attachment of the HVE was only 1 cm away from the scaler tip, with a similar horizontal height. In this study, the suction flow rate can be controlled to be three levels: high-volume evacuation 300 L/min; medium-volume evacuation 150 L/min; low-volume evacuation 70 L/min. The real-life photo of the experimental setup is shown in Fig. 1.

The 2D PIV system was utilized to analyze how the HVE alters the risk profiles during ultrasonic scaling by analyzing the performance of the HVE from the droplet velocity, flow field characteristics, and particle removal efficiency. The PIV system consisted of Litron Nd: YAG Lasers with an energy output of 50 $mJ/pulse$ at the wavelength of 532 nm, a 2560 pixel × 1600 pixel resolution Dantec SpeedSense CMOS camera and a synchronizer. A laser light sheet was formed with 2 mm thickness when the laser beam passed through the cylindrical lens, and the automatic transverse gauge was utilized to change the location of the light sheet. The CMOS camera was positioned perpendicular to the illuminated plane.

Although the high-sensitive laser light scattering method could be used to identify the characteristics of the medium-sized (5 μm–100 μm) and larger (>100 μm) droplets [19]. However, to monitor the changes of the flow-field characteristics, like the vortex structures, the dimension of the field of view (FOV) had been increased to 670 mm × 418 mm. The design of experimental conditions was the compromise between the characteristic of the particle size range and the experimental resources, and the analyzed particle size was the larger droplets (>100 μm). The detailed parameter selection was presented in our previous studies [46]. In this study, three different suction flow rates (300 L/min, 150 L/min, and 70 L/min) were used throughout the ultrasonic scaling, and the experiment had been repeated three times to ensure accurate results and estimate the variability of the results. In each condition, the 200 sequential instantaneous velocity fields were measured at a sampling frequency of 40 Hz. The time between continuous pulses was calculated based on the estimated in-plane velocity and the size of the interrogation area to set 144 us. The experimental designs are based on the compromise between the experimental resources and better revelation of the performance of the HVE during ultrasonic scaling.

To tracking the emitted droplets, the image sequences were processed through several steps. Firstly, removing the background noise was through background noise subtraction. Next, the adaptive PIV method with a more precise subpixel interpolation scheme was selected to calculate the velocity vectors from the image sequences. The size of the interrogation area could adjust according to the local seeding density and flow gradient. The above data processing methods could reduce the error by less than 3.0% in the velocity field analysis [47]. The statistical analyses in this study were performed to find out the relationship between the suction flow rates and particle removal efficiency. Additionally, every 40 frames in one suction rate were extracted as a frame band to do the comparison. All the data were analyzed by the commercial package SPSS, version 22.0. The normality and homogeneity of variance of the obtained data would be checked for the selection of appropriate

Fig. 1. The real-life photo of the experimental setup.

statistical tests. The post-hoc tests would be performed if there were statistically significant differences between the particle removal efficiency in the three suction flow rates.

2.2. Proper orthogonal decomposition (POD) analysis

The Proper Orthogonal Decomposition (POD) analysis is widely used to evaluate the turbulent flow characteristics [48]. In this study, the POD analysis method is composed of two separated parts, taking a snapshot of instantaneous velocity field by PIV, and performing a series of analyses in the same position and under identical operating conditions. A detailed description of the calculation and analysis procedures are shown as follow:

Firstly, the mean velocity field, as the zeroth mode of POD, should be calculated from all snapshots. The fluctuating parts of velocity components (u_{mn}, v_{mn}) are obtained by subtracting the mean from all snapshots, which would be used for the rest analysis. The index ranges from 1 to M (total number of positions in the field), and n is from 1 to N (total number of snapshots).

Secondly, the time-space matrix **U** is constituted by obtaining all fluctuating velocity components from N snapshots, arranged as in equation (1). In the below matrix, each row is formed by the time series of specific velocity components in a specific point, and each column is composed of all velocity components in one snapshot.

$$U = \begin{bmatrix} u_{11} & u_{12} & \cdots & u_{1N} \\ \vdots & \vdots & \vdots & \vdots \\ u_{M1} & u_{M2} & \cdots & u_{MN} \\ v_{11} & v_{12} & \cdots & v_{1N} \\ \vdots & \vdots & \vdots & \vdots \\ v_{M1} & v_{M2} & \cdots & v_{MN} \end{bmatrix} \quad (1)$$

Thirdly, the N x N autocovariance matrix **R** is formed from matrix **U**.

$$\widetilde{R} = U^T U \quad (2)$$

And the corresponding eigenvalue can be obtained:

$$\widetilde{R}\varnothing_i = \lambda_i \varnothing_i \quad (3)$$

Where λ_i and $\varnothing_i$ are corresponding eigenvalue and eigenvectors, respectively. The ordered solution can be obtained by the size of corresponding eigenvalues.

$$\lambda_1 > \lambda_2 > \ldots > \lambda_N = 0 \quad (4)$$

The POD modes, also the normalized eigenfunctions, can be computed by combining eigenvalues and eigenvectors with the U matrix.

$$\phi_i = \frac{\sum_{n=1}^{N} \varnothing_i^n u_n}{\sum_{n=1}^{N} \varnothing_i^n u_n}, \ i = 1, \ldots, N, \quad (5)$$

Where $\varnothing_i^n$ is the nth eigenvector corresponding to eigenvalue λ_i. The normalization is defined by the discrete 2-norm.

$$y = \sqrt{y_1^2 + y_2^2 + \ldots + y_M^2} \quad (6)$$

From the above mathematical derivation process and snapshot analysis, we found that the kinetic energy from the velocity fluctuation is proportional to the corresponding calculated eigenvalue. The first mode usually accounts for the largest energy due to the order of eigenvalues and eigenvector, which is also associated with a large and dominant flow structure.

For the original PIV measured instantaneous flow fields, some traditional methods in fluid mechanics have shown some limitations in the detailed analysis of the flow characteristics like vortex identification [49]. In contrast, the POD analysis method could act as a 'filter' and reconstruct the flow field with specific turbulent kinetic energy. Generally, the lower modes account for large kinetic energy, and the higher modes are considered as the noise or random background information in the flow fields.

3. Results

3.1. The velocity profiles

Fig. 2 depicted the time-averaged velocity vector fields in the X–Y plane with three suction flow rates: 300 L/min, 150 L/min, and 70 L/min and controlled 0 L/min. For visual clarity, only half of the vectors were presented in the below figures. In other words, the actual spatial resolution of the obtained flow field was 4 times higher than that shown in Fig. 2. As plotted by the contour map of the velocity and vector presented in Fig. 2, the flow structures were generally similar: the airflow issuing from the operation site was in an obliquely upward
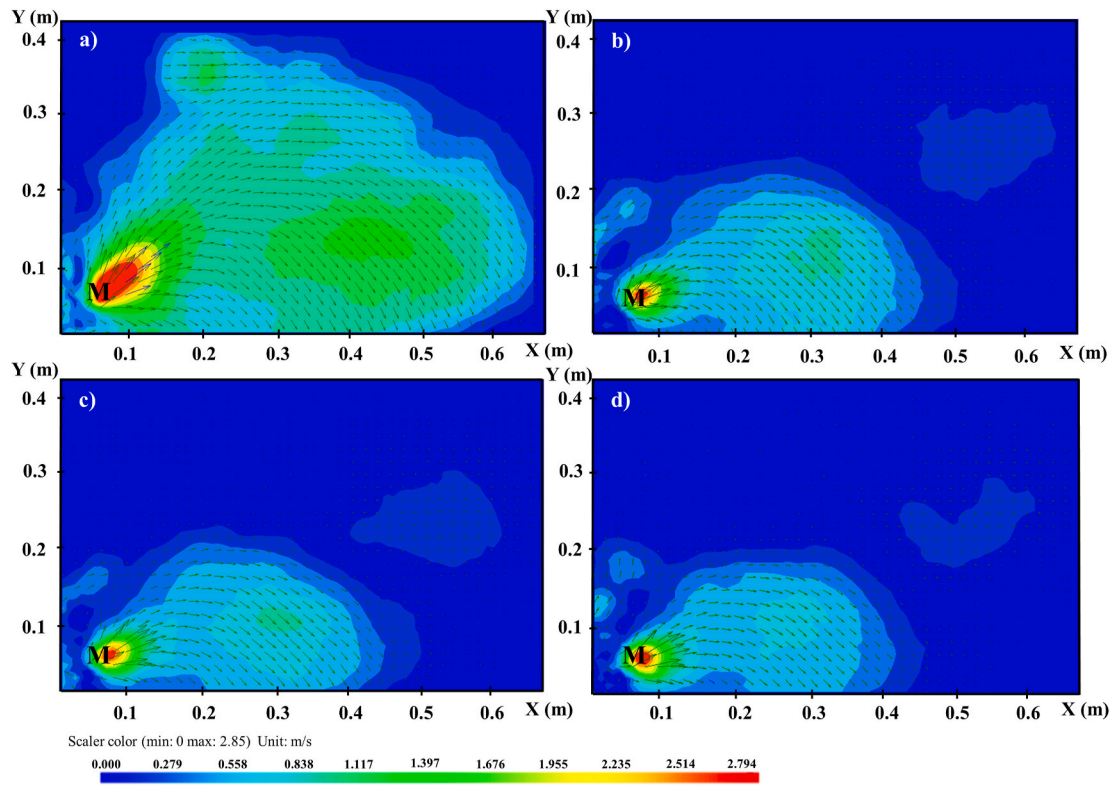
Fig. 2. The time-averaged velocity vector fields: a) No HVE_ 0 L/min; b) suction flow rate_300 L/min; c) suction flow rate_150 L/min; d) suction flow rate_70 L/min. The coordinates of the mannequin's mouth are (0.05 m, 0.05 m), referred to by "M".
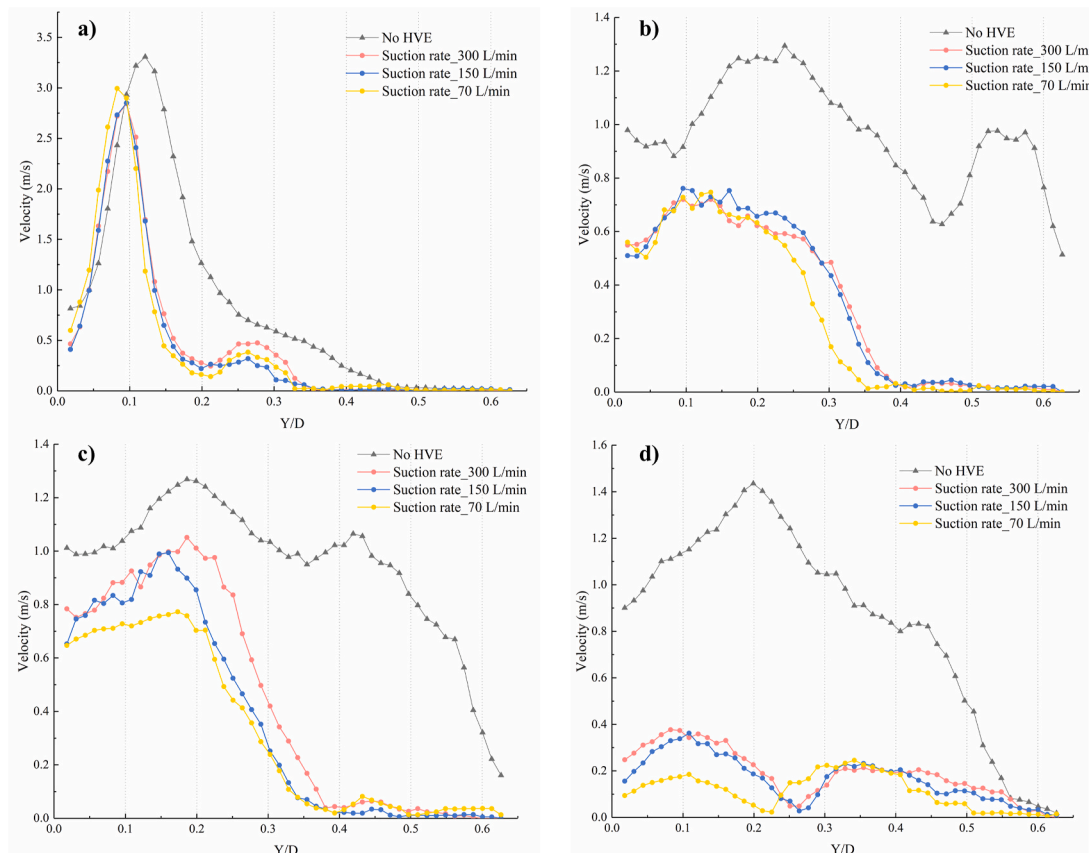
Fig. 3. The droplet velocity profiles for all cases: a) X = 0.1D; b) X = 0.3D; c) X = 0.5D; d) X = 0.7D.

direction. In Fig. 2a (without the cooperation of the HVE), the maximum velocity of the expelled droplet near the mannequin's mouth was in line with previous theoretical estimation, 3–4 m/s [50]. Besides, another high-velocity region was presented at the top of the FOV, and it may cause large, contaminated regions. In comparison with Fig. 2a, the flow pattern in Fig. 2b, c, and 2d charted the remarkable difference that the high-velocity region at the top of FOV disappeared, and the similar droplet velocity distribution was observed near the mannequin's mouth. The above observation referred that the cooperation of the HVE could not eliminate the droplet particles generated during ultrasonic scaling, but the suction can be characterized as low-threshold equipment to bring substantial benefits to reduce the area of the contaminated region.

To further investigate the HVE performance on the high-velocity droplets, the velocity profiles calculated by the $\sqrt{U^2 + V^2}$) at the relative location were presented in Fig. 3, with the four relative locations (X/D = 0.1, 0.3, 0.5, 0.7, D = 0.67 the length of X-axis). As shown in Fig. 3a, the velocity profiles were extracted near the mannequin's mouth, and the velocity distribution was generally in a similar trend. The velocity profiles of four different conditions at X/D = 0.1 showed that the peak velocity kept in the constant range (3.0–3.5 m/s) at almost the same location. The phenomenon could be accounted for by the moderate performance of the HVE on the high-velocity droplets, and the observation has proven the previous hypothesis about the effect of dental suction [27]. Since the high-velocity droplets would collide and even attach to the outer layer of the mask and clothes, other mitigation measures like the air purifier and external suction device may be used together to further reduce the exposure risks.

As presented in Fig. 3b, the obvious difference in velocity distribution was observed whether the cooperation of the HVE. The velocity profiles without the cooperation of the HVE at X/D = 0.3 exhibited an obvious bimodal distribution: the first peak velocity (1.2 m/s) near 0.15 < Y/D < 0.25, and the second one (1.0 m/s) near 0.5 < Y/D < 0.6. The phenomenon created was due to the turbulent clouds at the top of FOV, further constituted the large, contaminated region, and the detailed analysis would be presented in the following section 3.2. By contrast, the flow field and velocity profiles were totally different in the cooperation of the suction. Although there were different suction flow rates, all the velocity profiles exhibited a unimodal distribution, and a peak velocity presented in a similar location. Due to the above similar performance in the flow field, the low threshold for suction bringing significant benefit was further confirmed. Fig. 3c and d showed the gap of velocity profiles with and without the HVE became larger with the increased distance from the mannequin's mouth, further reduce the area of contaminated regions. A slight difference in the velocity profiles in various suction flow rates was observed partly due to the intervention between the ambient flow and the expelled airflow. Notably, although the low threshold for suction bringing significant benefit, the higher suction flow rates (300 L/min) could reduce the influence of ambient airflow and turbulence of wake flow than the lower suction rates (150 L/min and 70 L/min).

3.2. The risk profiles

3.2.1. The POD analysis

To further investigate the flow fields, the POD analysis was employed to investigate the fluctuation characteristics and determine their corresponding temporal features. Since the POD analysis could extract the different modes of the flow field based on the turbulence kinetic energy [51], the analysis method was widely used to excavate the domain structure of complex transient flow fields [52,53].

In order to identify the energy composition features, Fig. 4 presented the energy accumulation characteristics in modes under whether the cooperation of the dental suction device. Since the POD analysis was based on the fluctuating parts of velocity components (subtracting the mean velocity field), the overall increasing trends for the four conditions
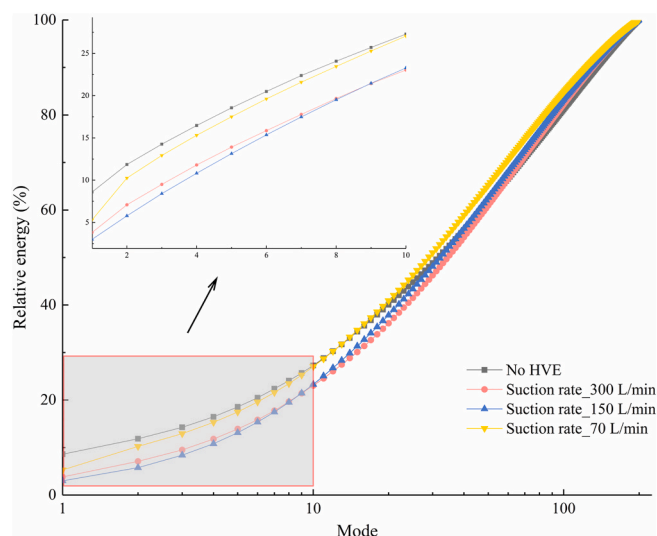

Fig. 4. The energy accumulation characteristics in modes with and without dental suction device.

were generally in line, but the lower modes still contributed more energy in the flow field. In order to make the quantitative comparison, the conditions of No HVE and suction flow rates 300 L/min were extracted: Mode 1 contributed 8.6%, and 3.8%, and the first 20 modes accounted for 40.1%, and 36.2% of total energy without and with the cooperation of the HVE, respectively. Whereas the energy of the flow field in the cooperation of the HVE had a relatively even distribution across modes, and the cumulative energy exceeded the condition of No HVE at mode 60. To cover 90% of the total energy of the flow field, the first 136 and 131 modes were selected to reconstruct the instantaneous flow field under the condition with and without HVE, respectively. Hence, more modes were needed to reconstruct an instantaneous flow field under the condition of No HVE. The above phenomenon indicated that smaller scale flow structures were contained in the flow field under the condition of No HVE than that of HVE operations.

The selected POD modes under whether the cooperation of the HVE (suction flow rate: 300 L/min) was presented in Fig. 5. A clear velocity distribution difference between different modes and the time-averaged one was observed. Among the first twenty modes that contributed around 40% of the total energy, Mode 1, and Mode 2 of both two conditions with and without the HVE operation were totally different. As for the condition of No HVE, the maximum velocity region existed at the top of FOV. In other words, the domain structure, Mode 1, and Mode 2 reflected the conjugated turbulence structures, and the observation was in line with previous results [46]. In contrast, under the condition with the HVE (300 L/min), Mode 1, and Mode 2 were composed of two high-velocity structures, which presented the movement tendency of droplet particles and contaminated regions (the head and chest areas of patients). Modes 3 and 4 of each condition were quite similar with several flow structures existing in the nearby regions. However, compared with the condition of No HVE, the flow structure in Modes 3 and 4 were more located at the bottom of FOV under the cooperation of the HVE, which further confirmed the significant performance of the HVE to reduce site contamination. From Mode 5 to Mode 20, the smaller and irregular coherent structures were presented, reflecting the fluctuation characteristics of the flow field. With the increasing of mode numbers, the flow structures were more random and irregular, and the relative energy contribution became lower. As shown in Fig. 5, the extracted Mode 100 and Mode 200 refereed the relatively random flows, which could be treated as the background noise.

3.2.2. The particle removal efficiency

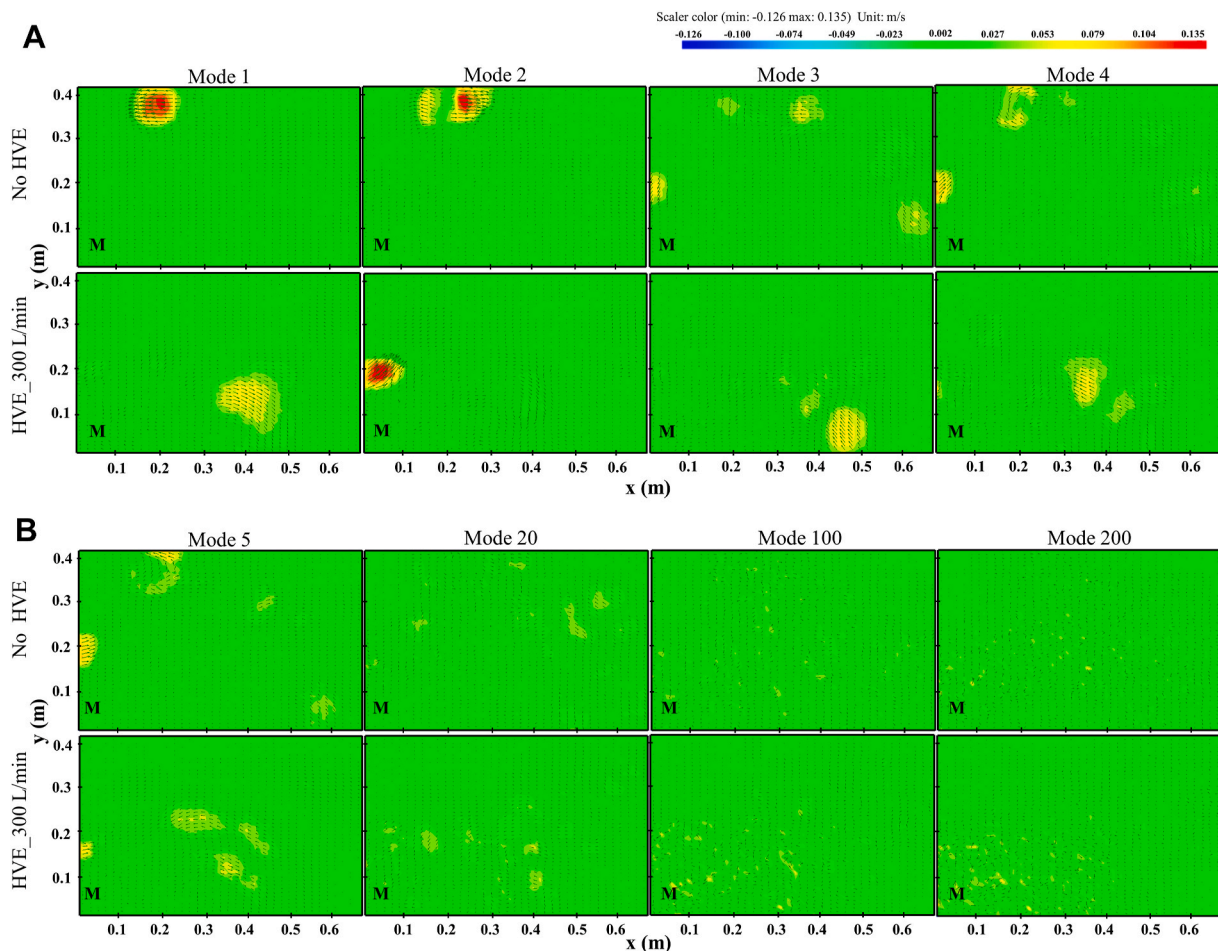To further evaluate the performance of HVE on the spatters gener-

Fig. 5. Typical POD modes of the fluctuation flow field under whether the cooperation of the HVE (300 L/min). The coordinates of the mannequin's mouth are (0.05 m, 0.05 m), referred to by "M".

ated during ultrasonic scaling, the recorded image sequences were analyzed frame by frame to determine the number of particles whose maximum single-pixel intensity exceeded 30 threshold values [54]. The particle removal efficiency ($\phi = 1 - n_1/n_0$) was proposed to compare the performance of the HVE at different suction flow rates. To avoid the fluctuation of particles in each image, n_1 and n_0 referred the average number of detected particles in every forty images (time step: 1 s) in three suction flow rates and No HVE, respectively.

Although the normality of the data of the particle removal efficiency in the three suction flow rates was verified by the Shapiro-Wilk Tests, the variance of the three data sets was found to be non-homogeneity. Therefore, non-parametric tests (Kruskal-Wallis tests and Mann–Whitney U tests) were conducted to test the difference between the data. In the results of Kruskal-Wallis tests, the median of the particle removal efficiency between the three suction flow rates ($ps < 0.05$) were found to be statistically different in the 2nd, 3rd, and 5th frame bands (see Fig. 6). The results of the post-hoc tests for the data in these three frame bands were also shown in Fig. 6.

Considering that the number of suspended particles in the operation room increased as the operation time went on, variations of the particle removal efficiency of dental suction among the three conditions were observed. However, the cooperation of dental suction could significantly decrease the number of expelled particles. Compared with other conditions, the efficiency of HVE in 300 L/min was more stable, at around 60%. For both dental suction flow rates 150 L/min and 70 L/min, the averaged efficiency varied in the range of 49%–53%. The above-obtained results were generally in line with previous results, which measured the settled contaminated area on filter paper (reducing 53%)
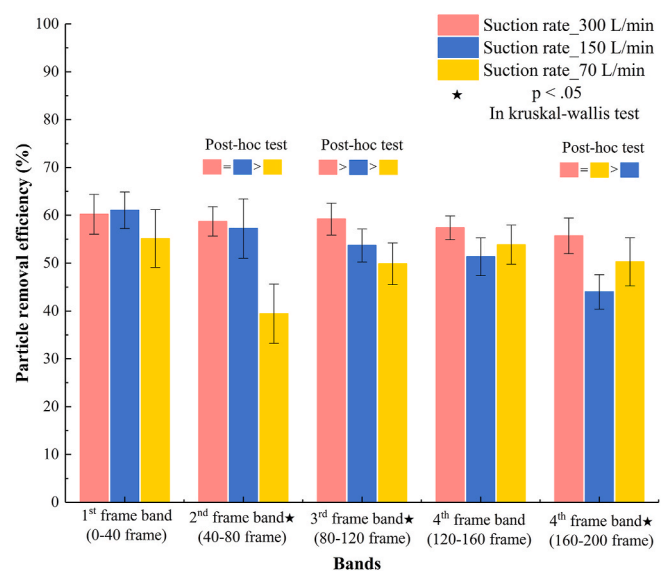

Fig. 6. The particle removal efficiencies among three suction flow rates (suction flow rates: 300 L/min, 150 L/min, and 70 L/min).

under medium and low volume suction [27]. The corresponding images recorded by a high-speed camera under four conditions were also presented in Fig. 7. Notably, although there are no studies that reported that
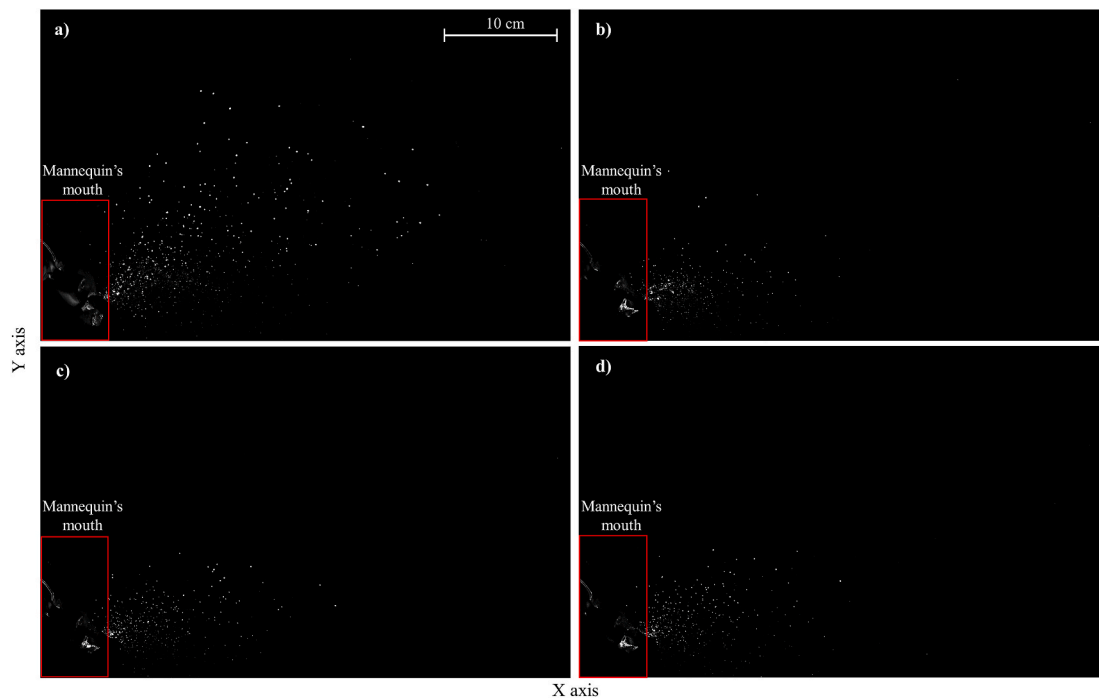
Fig. 7. The corresponding images under four conditions: a) No HVE; b) suction flow rate_300 L/min; c) suction flow rate_150 L/min; d) suction flow rate_70 L/min. The images were retrieved from the first frame of each image sequence, and the visualization comparison of Fig. 7a and b was in the supplementary video.

one piece of equipment could 100% eliminate the emitted droplets and aerosols, the integrated use of other equipment could help to further reduce the exposure risk of dental professionals and patients.

4. Discussion

Dental aerosols and fluid droplets generated during dental procedures may cause the cross-transmission of SARS-CoV-2 among dental professionals and patients. Several questions about the suspended particles should be addressed: Question 1: how long do the particles remain airborne in the dental surgery operation room? The fallow time has been proposed and defined as when the number of suspended particles drops to the level that the next patient can safely enter after the aerosol-generating procedures (AGPs) [55]. Some studies have proven that the duration of around 30-min after the procedure is enough for the next patients in the environment with 6 ACH [27,56]. Question 2: how far do the expelled particles from dental procedures be transmitted? Allison et al. found that a high-speed air-turbine produced particles that transmit 4 m from the operative site [42], and that may contribute to the combined effect of the turbulence cloud and the ventilation airflow [57]. Li et al. found that the high-level contaminated region was within 1 m of the oral cavity by the PIV measurement [46]. Question 3: currently, various mitigation measures have been recommended in the dental guideline document, and how this equipment alters the risk profile in comparison with the situation where only masks, face shields, and other PPE? In the present study, we focused on the third question. Holliday et al. hypothesized that the effect of the HVE on high-velocity droplets or large droplets was moderate, although could be significantly helpful to reduce the area of the contaminated region [27]. The operation of AGPs in the dental surgery operation room could generate the high-velocity small droplets and aerosols which played a critical role in the cross-transmission [58]. These particles could not only be suspended for a quite long time but also collide and even attach to the outer layer of the mask and clothes. To mitigate the potential contamination of fluid droplets and aerosols generated, the Hong Kong Center for Health Protection highly recommended using the HVE during dental services. The present study confirmed the previous hypothesis about the moderate

effect of the HVE on the high-velocity small droplets by comparing the velocity profiles. Therefore, to further reduce the risk, other mitigation measures like the air filter may be used together.

Although several studies intended to evaluate the performance of the HVE by measuring the contamination region [39,43] and concentration of suspended particles [17,40], to the best of our knowledge, this is the first study to provide the quantitative evidence and analysis from the flow-field, size and velocity distribution of particles in the dental clinic. In this study, the emitted droplets were tracked and captured by the high-speed CMOS camera when the ultrasonic scaling was performed. In the condition of No HVE, a pair of vortexes was presented in the top left of the field of view (in Fig. 5), with the coordinates of (0.15 m,0.4 m). The relative vertical distance between the mannequin's mouth and the vortexes is about 0.35–0.4 m, which was in line with the recommended distance from the dental professional's eye to the patient oral cavity [59]. Compared with the condition of No HVE, a pair of vortexes located in the face shield area of the dental professional disappeared. The small droplets circulated in the turbulence vortexes would cause high-level contamination, which has already been confirmed by previous studies [60]. So, the cooperation of HVE could help to eliminate the turbulence vortexes in the dental surgery operation room, change the high-level contaminated region near the breathing area of dental professionals and even reduce the fallow time.

Currently, the aerodynamic particle sizer (APS) is widely used to perform real-time aerosol analysis and is best suited for particles ranging from 0.05 to 10 μm, which is well outside the range observed by laser light scattering [61]. The high sensitivity of the laser light scattering method can be used to investigate the medium-sized (10–100 μm) droplets and larger (>100 μm) droplets [54]. The laser light scattering, and APS methods could form a perfect complement. Based on the observation of numerous airborne particles during dental procedures, the current PPE plays a critical role to prevent potential transmission. Although the performance of the HVE device has been detected, it should be noted that the HVE device, as other mitigation measures, cannot completely eliminate the risk profile to dental professionals, around 60% of particle removal efficiency. It was quite critical to minimize these risks as much as possible.

The limitation of the study includes the absence of dental procedures in real patients. Although the volume of saliva is significantly less than that of cooling water during ultrasonic scaler, some biological materials in the saliva might affect the size and even velocity distribution of the emitted particles. More aerosol-generating procedures should be considered in future research, not only for ultrasonic scaling.

5. Conclusion

In summary, the study quantitatively evaluated how the HVE alters the risk profiles during ultrasonic scaling by analyzing the performance of the HVE from the droplet velocity, flow field characteristics, and particle removal efficiency. Moreover, this study not only provides high-quality data for CFD validation but also provides evidence for the dental recommendation:

a) From the results of the velocity profiles, the hypothesis about the moderate effect of the HVE on high-velocity droplets near the mannequin's mouth had been firstly proven in this study. The suction can be characterized as low-threshold equipment to bring substantial benefits to reduce the area of the contaminated region.
b) From POD analysis about the multi-scale characteristics of the airflow, once the cooperation of suction, the pair of vortexes that were in the face shield area of the dental professional would be eliminated, removing the high-level contaminated region near the breathing area of dental professionals.
c) The statistically significant differences between the particle removal efficiency in the three suction flow rates was observed, and the efficiency of the HVE with 300 L/min was more stable at 60%.

Declaration of competing interest

The authors declare that they have no known competing financial interests or personal relationships that could have appeared to influence the work reported in this paper.

Appendix A. Supplementary data

Supplementary data to this article can be found online at https://doi.org/10.1016/j.buildenv.2021.108225.

References

[1] X. Li, Y. Wei, J. Zhang, P. Jin, Design and analysis of an active daylight harvesting system for building, Renew. Energy 139 (2019) 670–678.
[2] C. Tung, C. Mak, J. Niu, K. Hung, Y. Wu, N. Tung, H. Wong, Enlightenment of re-entry airflow: the path of the airflow and the airborne pollutants transmission in buildings, Build. Environ. 195 (2021) 107760.
[3] Z.-y. Ge, L.-m. Yang, J.-j. Xia, X.-h. Fu, Y.-z. Zhang, Possible aerosol transmission of COVID-19 and special precautions in dentistry, J. Zhejiang Univ. - Sci. B (2020) 1–8.
[4] M. Jamal, M. Shah, S.H. Almarzooqi, H. Aber, S. Khawaja, R. El Abed, Z. Alkhatib, L.P. Samaranayake, Overview of transnational recommendations for COVID-19 transmission control in dental care settings, Oral Dis. 27 (2021) 655–664.
[5] C.F.H.P.H. Kong, Coronavirus disease (COVID-19) - letters to dentists, 2020 from, https://www.chp.gov.hk/files/pdf/letters_to_dentists_200128.pdf. for Coronavirus disease (COVID-19)—Letters to Dentists..
[6] Z. Ai, C.M. Mak, N. Gao, J. Niu, Tracer Gas Is a Suitable Surrogate of Exhaled Droplet Nuclei for Studying Airborne Transmission in the Built Environment. Building Simulation, Springer, 2020.
[7] X. Peng, X. Xu, Y. Li, L. Cheng, X. Zhou, B. Ren, Transmission routes of 2019-nCoV and controls in dental practice, Int. J. Oral Sci. 12 (1) (2020) 1–6.
[8] W. Alhazzani, M.H. Møller, Y.M. Arabi, M. Loeb, M.N. Gong, E. Fan, S. Oczkowski, M.M. Levy, L. Derde, A. Dzierba, Surviving Sepsis Campaign: guidelines on the management of critically ill adults with Coronavirus Disease 2019 (COVID-19), Intensive Care Med. (2020) 1–34.
[9] J. Korth, B. Wilde, S. Dolff, O.E. Anastasiou, A. Krawczyk, M. Jahn, S. Cordes, B. Ross, S. Esser, M. Lindemann, SARS-CoV-2-specific antibody detection in healthcare workers in Germany with direct contact to COVID-19 patients, J. Clin. Virol. 128 (2020) 104437.
[10] N. Van Doremalen, T. Bushmaker, D.H. Morris, M.G. Holbrook, A. Gamble, B. N. Williamson, A. Tamin, J.L. Harcourt, N.J. Thornburg, S.I. Gerber, Aerosol and surface stability of SARS-CoV-2 as compared with SARS-CoV-1, N. Engl. J. Med. 382 (16) (2020) 1564–1567.
[11] G. Kampf, D. Todt, S. Pfaender, E. Steinmann, Persistence of coronaviruses on inanimate surfaces and their inactivation with biocidal agents, J. Hosp. Infect. 104 (3) (2020) 246–251.
[12] H. Xu, L. Zhong, J. Deng, J. Peng, H. Dan, X. Zeng, T. Li, Q. Chen, High expression of ACE2 receptor of 2019-nCoV on the epithelial cells of oral mucosa, Int. J. Oral Sci. 12 (1) (2020) 1–5.
[13] R. Yan, Y. Zhang, Y. Li, L. Xia, Y. Guo, Q. Zhou, Structural basis for the recognition of SARS-CoV-2 by full-length human ACE2, Science 367 (6485) (2020) 1444–1448.
[14] N. An, L. Yue, B. Zhao, Droplets and aerosols in dental clinics and prevention and control measures of infection, Zhonghua Kou Qiang Yi Xue Za Zhi= Zhonghua Kouqiang Yixue Zazhi= Chinese, journal of stomatology vol. 55 (2020). E004-E004.
[15] R. Izzetti, M. Nisi, M. Gabriele, F. Graziani, COVID-19 transmission in dental practice: brief review of preventive measures in Italy, J. Dent. Res. 99 (9) (2020) 1030–1038.
[16] K.A. Prather, L.C. Marr, R.T. Schooley, M.A. McDiarmid, M.E. Wilson, D.K. Milton, Airborne transmission of SARS-CoV-2, Science 370 (6514) (2020) 303–304.
[17] A. Nulty, C. Lefkaditis, P. Zachrisson, Q. Van Tonder, R. Yar, A clinical study measuring dental aerosols with and without a high-volume extraction device, Br. Dent. J. (2020) 1–8.
[18] T. Ehtezazi, D.G. Evans, I.D. Jenkinson, P.A. Evans, V.J. Vadgama, J. Vadgama, F. Jarad, N. Grey, R.P. Chilcott, SARS-CoV-2: characterisation and mitigation of risks associated with aerosol generating procedures in dental practices, Br. Dent. J. (2021) 1–7.
[19] P. Mirbod, E.A. Haffner, M. Bagheri, J.E. Higham, Aerosol formation due to a dental procedure: insights leading to the transmission of diseases to the environment, J. R. Soc. Interface 18 (176) (2021) 20200967.
[20] P. Bahl, C.M. de Silva, A.A. Chughtai, C.R. MacIntyre, C. Doolan, An experimental framework to capture the flow dynamics of droplets expelled by a sneeze, Exp. Fluid 61 (8) (2020) 1–9.
[21] K.L. Chong, C.S. Ng, N. Hori, R. Yang, R. Verzicco, D. Lohse, Extended lifetime of respiratory droplets in a turbulent vapor puff and its implications on airborne disease transmission, Phys. Rev. Lett. 126 (3) (2021), 034502.
[22] W. Zhang, C.M. Mak, H. Wong, Pollutant dispersion in a natural ventilated dental clinic, Build. Serv. Eng. Technol. 34 (3) (2013) 245–258.
[23] N. Mao, C. An, L. Guo, M. Wang, L. Guo, S. Guo, E. Long, Transmission risk of infectious droplets in physical spreading process at different times: a review, Build. Environ. (2020) 107307.
[24] Y. Ren, C. Feng, L. Rasubala, H. Malmstrom, E. Eliav, Risk for dental healthcare professionals during the COVID-19 global pandemic: an evidence-based assessment, J. Dent. 101 (2020) 103434.
[25] Y. Liu, Z. Ning, Y. Chen, M. Guo, Y. Liu, N.K. Gali, L. Sun, Y. Duan, J. Cai, D. Westerdahl, Aerodynamic analysis of SARS-CoV-2 in two Wuhan hospitals, Nature 582 (7813) (2020) 557–560.
[26] L. Setti, F. Passarini, G. De Gennaro, P. Barbieri, M.G. Perrone, M. Borelli, J. Palmisani, A. Di Gilio, V. Torboli, F. Fontana, SARS-Cov-2RNA found on particulate matter of Bergamo in Northern Italy: first evidence, Environ. Res. 188 (2020) 109754.
[27] R. Holliday, J.R. Allison, C. Currie, D. Edwards, C. Bowes, K. Pickering, S. Reay, J. Durham, N. Rostami, J. Coulter, Evaluating dental aerosol and splatter in an open plan clinic environment: implications for the COVID-19 pandemic, 2020.
[28] C. Zemouri, C. Volgenant, M. Buijs, W. Crielaard, N. Rosema, B. Brandt, A. Laheij, J. De Soet, Dental aerosols: microbial composition and spatial distribution, J. Oral Microbiol. 12 (1) (2020) 1762040.
[29] S.E. Chatoutsidou, A. Saridaki, L. Raisi, E. Katsivela, G. Tsiamis, M. Zografakis, M. Lazaridis, Airborne particles and microorganisms in a dental clinic: variability of indoor concentrations, impact of dental procedures, and personal exposure during everyday practice, Indoor Air (2021).
[30] S.R. Rasaiah, J. Allison, D.C. Edwards, Endodontic procedures produce bacterial droplet contamination-but what about viruses? Evid. Base Dent. 22 (2) (2021) 76–77.
[31] P.S. Kumar, K. Subramanian, Demystifying the mist: sources of microbial bioload in dental aerosols, J. Periodontol. 91 (9) (2020) 1113–1122.
[32] A. Meethil, S. Saraswat, P. Chaudhary, S. Dabdoub, P. Kumar, Sources of SARS-CoV-2 and other microorganisms in dental aerosols, J. Dent. Res. (2021), 00220345211015948.
[33] C.G. Estrich, M. Mikkelsen, R. Morrissey, M.L. Geisinger, E. Ioannidou, M. Vujicic, M.W. Araujo, Estimating COVID-19 prevalence and infection control practices among US dentists, J. Am. Dent. Assoc. 151 (11) (2020) 815–824.
[34] B. Chanpong, M. Tang, A. Rosenczweig, P. Lok, R. Tang, Aerosol-generating procedures and simulated cough in dental anesthesia, Anesth. Prog. 67 (3) (2020) 127–134.

[35] M. Mupparapu, Aerosol reduction urgency in post-COVID-19 dental practice, Quintessence Int Berl Ger 51 (7) (2020).

[36] Z. Ai, C.M. Mak, H. Wong, Noise level and its influences on dental professionals in a dental hospital in Hong Kong, Build. Serv. Eng. Technol. 38 (5) (2017) 522–535.

[37] K.W. Ma, H.M. Wong, C.M. Mak, Dental environmental noise evaluation and health risk model construction to dental professionals, Int. J. Environ. Res. Publ. Health 14 (9) (2017) 1084.

[38] K.W. Ma, H.M. Wong, C.M. Mak, A systematic review of human perceptual dimensions of sound: meta-analysis of semantic differential method applications to indoor and outdoor sounds, Build. Environ. 133 (2018) 123–150.

[39] S.E. Chavis, S.E. Hines, D. Dyalram, N.C. Wilken, R.N. Dalby, Can extraoral suction units minimize droplet spatter during a simulated dental procedure? J. Am. Dent. Assoc. 152 (2) (2021) 157–165.

[40] M. Yang, A. Chaghtai, M. Melendez, H. Hasson, E. Whitaker, M. Badi, L. Sperrazza, J. Godel, C. Yesilsoy, M. Tellez, Mitigating saliva aerosol contamination in a dental school clinic, BMC Oral Health 21 (1) (2021) 1–8.

[41] J. Balanta-Melo, A. Gutiérrez, G. Sinisterra, M.d.M. Díaz-Posso, D. Gallego, J. Villavicencio, A. Contreras, Rubber dam isolation and high-volume suction reduce ultrafine dental aerosol particles: an experiment in a simulated patient, Appl. Sci. 10 (18) (2020) 6345.

[42] J.R. Allison, C.C. Currie, D.C. Edwards, C. Bowes, J. Coulter, K. Pickering, E. Kozhevnikova, J. Durham, C.J. Nile, N. Jakubovics, Evaluating aerosol and splatter following dental procedures: addressing new challenges for oral health care and rehabilitation, J. Oral Rehabil. 48 (1) (2021) 61–72.

[43] S. Shahdad, T. Patel, A. Hindocha, N. Cagney, J.-D. Mueller, N. Seoudi, C. Morgan, A. Din, The efficacy of an extraoral scavenging device on reduction of splatter contamination during dental aerosol generating procedures: an exploratory study, Br. Dent. J. (2020) 1–10.

[44] P. Anfinrud, V. Stadnytskyi, C.E. Bax, A. Bax, Visualizing speech-generated oral fluid droplets with laser light scattering, N. Engl. J. Med. 382 (21) (2020) 2061–2063.

[45] P. Bahl, S. Bhattacharjee, C. de Silva, A.A. Chughtai, C. Doolan, C.R. MacIntyre, Face coverings and mask to minimise droplet dispersion and aerosolisation: a video case study, Thorax 75 (11) (2020) 1024–1025.

[46] X. Li, C.M. Mak, K.W. Ma, H.M. Wong, Evaluating flow-field and expelled droplets in the mockup dental clinic during the COVID-19 pandemic, Phys. Fluids 33 (4) (2021), 047111.

[47] X. Cao, J. Liu, N. Jiang, Q. Chen, Particle image velocimetry measurement of indoor airflow field: a review of the technologies and applications, Energy Build. 69 (2014) 367–380.

[48] L. Sirovich, Turbulence and the dynamics of coherent structures. II. Symmetries and transformations, Q. Appl. Math. 45 (1987) 573–582.

[49] J. Li, J. Liu, C. Wang, M. Wesseling, D. Müller, PIV experimental study of the large-scale dynamic airflow structures in an aircraft cabin: swing and oscillation, Build. Environ. 125 (2017) 180–191.

[50] J. Plog, J. Wu, Y.J. Dias, F. Mashayek, L.F. Cooper, A.L. Yarin, Reopening dentistry after COVID-19: complete suppression of aerosolization in dental procedures by viscoelastic Medusa Gorgo, Phys. Fluids 32 (8) (2020), 083111.

[51] Y. Wei, T.T. Zhang, S. Wang, Prompt design of the air-supply opening size for a commercial airplane based on the proper orthogonal decomposition of flows, Build. Environ. 96 (2016) 131–141.

[52] B. Kim, K.T. Tse, A. Yoshida, Z. Chen, P. Van Phuc, H.S. Park, Investigation of flow visualization around linked tall buildings with circular sections, Build. Environ. 153 (2019) 60–76.

[53] S. Yin, Y. Fan, M. Sandberg, Y. Li, PIV based POD analysis of coherent structures in flow patterns generated by triple interacting buoyant plumes, Build. Environ. 158 (2019) 165–181.

[54] V. Stadnytskyi, C.E. Bax, A. Bax, P. Anfinrud, The airborne lifetime of small speech droplets and their potential importance in SARS-CoV-2 transmission, Proc. Natl. Acad. Sci. Unit. States Am. 117 (22) (2020) 11875–11877.

[55] L. Xiujie, C.M. Mak, K.W. Ma, H.M. Wong, Restoration of dental services after COVID-19: the fallow time determination with laser light scattering, Sustainable Cities and Society (2021) 103134.

[56] N. Raghava, B. Vidovic, Using computational fluid dynamics to evaluate the role of air purification in reducing fallow time in dentistry, 2020.

[57] L. Bourouiba, Turbulent gas clouds and respiratory pathogen emissions: potential implications for reducing transmission of COVID-19, Jama 323 (18) (2020) 1837–1838.

[58] J. Komperda, A. Peyvan, D. Li, B. Kashir, A.L. Yarin, C.M. Megaridis, P. Mirbod, I. Paprotny, L.F. Cooper, S. Rowan, Computer simulation of the SARS-CoV-2 contamination risk in a large dental clinic, Phys. Fluids 33 (3) (2021), 033328.

[59] M.A. Aldosari, Dental magnification loupes: an update of the evidence, J. Contemp. Dent. Pract. 22 (3) (2021) 310–315.

[60] N. Innes, I. Johnson, W. Al-Yaseen, R. Harris, R. Jones, S. Kc, S. McGregor, M. Robertson, W. Wade, J.E. Gallagher, A systematic review of droplet and aerosol generation in dentistry, J. Dent. (2020) 103556.

[61] B. Polednik, Exposure of staff to aerosols and bioaerosols in a dental office, Build. Environ. 187 (2021) 107388.